Journal of Colloid and Interface Science 449 (2015) 205–214

Contents lists available at ScienceDirect

Journal of Colloid and Interface Science

www.elsevier.com/locate/jcis

# Surfactants with colloids: Adsorption or absorption?

Gregory N. Smith [a], Isabelle Grillo [b], Sarah E. Rogers [c], Julian Eastoe [a,*]

[a] School of Chemistry, University of Bristol, Cantock's Close, Bristol BS8 1TS, United Kingdom
[b] Institut Max-von-Laue-Paul-Langevin, BP 156-X, F-38042 Grenoble Cedex, France
[c] ISIS-STFC, Rutherford Appleton Laboratory, Chilton, Oxon OX11 0QX, United Kingdom

## GRAPHICAL ABSTRACT

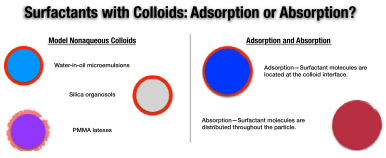


## ARTICLE INFO

*Article history:*
Received 23 October 2014
Accepted 8 December 2014
Available online 2 February 2015

*Keywords:*
Colloids
Small-angle neutron scattering
Nonpolar solvents

## ABSTRACT

*Hypothesis:* The interaction of Aerosol OT (AOT) surfactant with systems of model colloids in nonaqueous solvents (water-in-oil microemulsions, surfactant-stabilized silica organosols, and sterically-stabilized PMMA latexes) is expected to be system specific. Two limiting cases are expected: adsorption, with surfactant located at the particle surfaces, or absorption, with surfactant incorporated into the particle cores.
*Experiments:* Two approaches have been used to determine how AOT is distributed in the colloidal systems. The stability of the colloids in different alkanes (heptane to hexadecane, including mixtures) has been studied to determine any effects on the colloid surfaces. Contrast-variation small-angle neutron scattering (SANS) measurements of the colloid cores and of AOT-colloid mixtures in colloid-matched solvent have also been performed. Normalization to account for the different scattering intensities and different particle radii have been used to enable a system-independent comparison.
*Findings:* AOT in water-in-oil microemulsions and surfactant-stabilized silica organosols is determined to be adsorbed, whereas, surprisingly, AOT in sterically-stabilized PMMA latexes is found to be absorbed. Possible origins of these differences are discussed.


## 1. Introduction

Colloids in nonpolar solvents are crucial in many industries and applications; this motivates the extensive research into their properties. For example, water-in-oil microemulsions can be used as "nanoreactors" to produce many types of nanoparticles [1]; metal carbonate colloids have been used as lubricant detergents [2,3]; charged colloids can form crystal structures, which can be studied on a microscopic scale [4,5]. Charged species, in particular, which are not as easily stabilized in nonpolar solvents as in water, are important in many applications [6,7], such as preventing explosions in petrochemical processing [8] and, recently, in electrophoretic displays [9–11]. Novotny reviewed the applications of nonaqueous colloids, identifying four technologies making significant use of such systems: magnetic recording media, ceramics in electronic components, reprographic printing, and electrophoretic displays [12]. These high technology applications show the importance of colloids in nonpolar solvents.

Due to the properties of nonpolar solvents, the interparticle interactions are reduced as compared to aqueous colloids. In particular, unless charging agents are added, there is little electrostatic interaction between colloids, a consequence of the reduced relative permittivity ($\epsilon_r \approx 2$ for alkanes compared to $\epsilon_r = 80.1$ for water

* Corresponding author.
*E-mail address:* julian.eastoe@bristol.ac.uk (J. Eastoe).

http://dx.doi.org/10.1016/j.jcis.2014.12.048
0021-9797/

[13]). This can be seen from analyses of small-angle neutron scattering (SANS) data of such colloids where there is little contribution from the structure factor ($S(Q)$) in the dilute limit, indicating that the colloids are uncorrelated, weakly interacting, and randomly dispersed [14–16]. Colloids in nonpolar solvents can be considered to behave as essentially model, hard spheres. For example, water-in-oil microemulsions only show attractions as the phase-separation boundary is approached [17], and sterically-stabilized polymer latexes show fluid, crystal, and glass phases which can be described by an effective hard-sphere model [18].

Given the importance of colloids in nonpolar solvents, in terms of both fundamental and applied research, it is worthwhile to improve understanding of their properties and structures. In this article, different model systems of colloids with a typical added surfactant (Aerosol OT or AOT) will be considered. As multicomponent systems, the role and distribution of each component is not as clear initially. There are three systems of interest.

- Water-in-oil microemulsions—These are thermodynamically stable dispersions of water in oil with surfactant [19].
- Surfactant-stabilized silica organosols—"Organosol" is a well-known term in colloid science used to denote inorganic nanoparticles that are stable dispersed in organic solvents [20].
- Sterically-stabilized poly(methyl methacrylate) (PMMA) latexes—These particles were initially developed in the 1980s [21]. They consist of PMMA cores, coated with aliphatic poly(12-hydroxystearic acid) (PHSA) brushes to provide steric stabilization.

This paper will assess the nature of the surfactant layer in these three systems. Is there evidence for adsorption on the surfaces, or on the other hand, is there evidence for absorption into the colloid cores? Fig. 1 shows a schematic of the two scenarios. In this study, adsorption is defined as the localization of the added surfactant at the colloid-solvent interfaces; absorption is defined as the distribution of the added surfactant throughout the particles.

Two approaches have been used to determine how AOT is distributed in these three model colloid systems. The effect of varying the solvent molecular volume on the stability of the dispersions reveals how effective the surfactant layer is in providing stability. There has been some previous work into the effect of different solvents on water-in-oil microemulsions [22,23] and surfactant-stabilized silica organosols [15,24]. There have been no systematic studies on the effect of different solvents on PMMA latexes, but they have been used in various organic solvents in different studies [25–28]. Additionally, SANS is used to reveal the distribution of surfactant in these different systems. By using appropriate normalization, it is possible to draw comparisons between these colloids ranging in size from $\sim 1$ to $\sim 100$ nm.

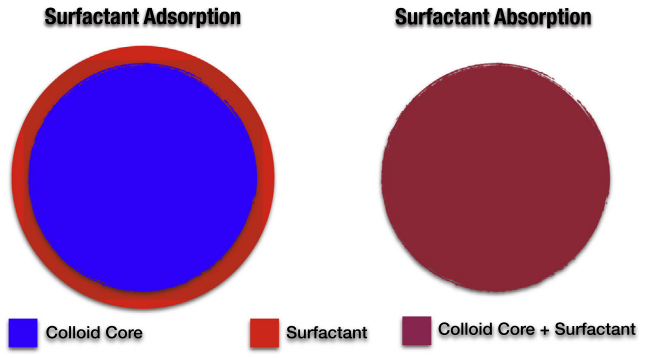


**Fig. 1.** Schematic of the distribution of surfactant in the two limiting cases: adsorption and absorption.

By considering the results of these two studies, it is possible to determine whether surfactant adsorption or surfactant absorption occurs for the three different systems. Some features are universal, whereas some features depend on properties of the particles. This provides insight into the mechanism by which surfactants, in general, and AOT, in particular, both stabilize and interact with colloids in nonpolar solvents.

## 2. Materials and methods

Sodium dioctylsulfosuccinate (Aerosol OT or AOT, 98%, Aldrich) was initially purified using dry diethyl ether followed by centrifugation to remove undissolved salts. Klebosol 30CAL25 (a gift from AZ Electronic Materials, France) was provided as a 30 wt.% dispersion in water. Heptane (CHROMASOLV $\geqslant$ 99%, Sigma–Aldrich), octane (97% pure, Acros Organics), dodecane (ReagentPlus $\geqslant$ 99%, Sigma–Aldrich), tetradecane (99%, Acros Organics), and hexadecane (minimum 99%, Sigma) were all stored over molecular sieves. Deuterium-labeled heptane-$d_{16}$ ($>$ 99.0 atom % D, Apollo Scientific) and dodecane-$d_{26}$ ($>$ 98%, Cambridge Isotope Laboratories) were used as supplied.

### 2.1. Silica organosols

Silica organosols were prepared using the drying method of Tabor et al. [15]. AOT surfactant was dissolved in water and combined with the required amount of 30CAL25. The 30CAL25 silica particles used in this study were positively charged in water with an electrophoretic mobility of $(2.1 \pm 0.2) \times 10^{-8}\ m^2\ V^{-1}\ s^{-1}$, measured using phase-analysis light scattering. The positive charge arises from alumina surface modification. The dispersions were mixed under sonication for 30 min; then the water was evaporated under vacuum at 60 °C for 12 h. The organic solvent mixture was added, and the dispersions were mixed under sonication for 30 min.

Unstable aggregates were removed by gently centrifuging the dispersions for 5 min at 3000 rpm. The sediment was dried under vacuum at 70 °C for 2 h to remove organic solvent. The transfer efficiency ($E$) was calculated by converting the mass of the sediment after gentle centrifugation to the mass remaining dispersed and divided by the mass of the solid before adding organic solvent.

### 2.2. PMMA latexes

PMMA latexes (as a dispersion in dodecane) were a gift from Merck Chemicals Ltd. and were prepared using the method described by Antl et al. [21]. The steric stabilizer was a graft copolymer with poly(12-hydroxystearic acid) (PHSA) brushes [29]. The solvodynamic diameter in dodecane is $392 \pm 4$ nm with a polydispersity index of 0.06, measured by dynamic light scattering (Malvern ZetaSizer Nano S90, Malvern, U.K.).

The latexes were transferred to octane and hexadecane by centrifuging the dispersions for 10 min at 6000 rpm and then redispersing in the desired alkane. This was repeated three times.

### 2.3. Small-angle neutron scattering (SANS)

Neutron scattering measurements were performed at both at the ISIS Pulsed Neutron Source (STFC Rutherford Appleton Laboratory, Didcot, U.K.) and the Institut Laue-Langevin (Grenoble, France). The magnitude of the momentum transfer vector ($Q$) is defined in Eq. (1), where $\theta$ is the scattering angle and $\lambda$ is the incident neutron wavelength.

$$Q = \frac{4\pi \sin\frac{\theta}{2}}{\lambda}. \quad (1)$$

Two instruments were used at ISIS. On Sans2d [30], two detector configurations were used. When using one detector, a simultaneous $Q$-range of 0.0045–0.7 Å$^{-1}$ was achieved utilizing an incident wavelength range of 1.75–16.5 Å and employing an instrument set up with source-sample and sample-detector distances of $L_1 = L_2 = 4$ m and the 1 m$^2$ detector offset vertically 60 mm and sideways −290 mm. When using two detectors, a simultaneous $Q$-range of 0.004–1.96 Å$^{-1}$ was achieved utilizing an incident wavelength range of 1.75–16.5 Å and employing an a collimation length of 4 m and the two 1 m$^2$ detectors arranged so that one was 4 m from the sample and offset vertically 60 mm and sideways 180 mm (small-angle detector) and the other was 2.4 m from the sample and offset 900 mm and rotated to face the sample (wide-angle detector). On LOQ [31], data were recorded on a single two-dimensional detector to provide a simultaneous $Q$-range of 0.008–0.24 Å$^{-1}$ utilizing neutrons with $2 \leqslant \lambda \leqslant 10$ Å. The beam diameter on both instruments was 8 mm. Each raw scattering data set was corrected for the detector efficiency, sample transmission and background scattering and converted to scattering cross-section data ($\partial\Sigma/\partial\Omega$ vs. $Q$) using the instrument-specific software, Mantid. These data were placed on an absolute scale (cm$^{-1}$) using the scattering from a standard sample (a solid blend of hydrogenous and perdeuterated polystyrene) in accordance with established procedures [32].

Measurements were also performed on D11 at the Institut Laue-Langevin. Two sample-detector distances of 1.2 and 8 m were used with collimation distances of 4 and 8 m. This gave an accessible $Q$-range of 0.004–0.3 Å$^{-1}$ at $\lambda = 10$ Å. The beam size was 7 mm × 10 mm; the data were placed on an absolute scale (cm$^{-1}$) by the measurement of a 1 mm thick sample of $H_2O$ as a standard.

The dispersions were contained in either 2 mm or 1 mm path length Hellma quartz cells as appropriate, depending on the level of D-labeled solvent.

Data have been fit to models as described in text using the SasView small-angle scattering analysis software package. Form factors ($P(Q)$) for spheres and core–shell spheres were used depending on the system being studied [33–35]. For spheres, the only variable parameter is the radius $r$. For core–shell spheres, the volume and the radius of the core ($V_c$ and $r_c$) and shell ($V_s$ and $r_s$) can vary, and contrasts between the core ($\rho_c$), the shell ($\rho_s$), and the solvent ($\rho_{solvent}$) must be considered. The fit radii values have a representative uncertainty of ±1 Å (considering repeat measurements and the use of different instruments) [36].

### 2.4. Phase-analysis light scattering (PALS)

Electrophoretic mobilities were measured using a Malvern Zetasizer Nano Z (Malvern, U.K.) with a universal dip cell electrode (for nonpolar solvents) or a disposable folded capillary cell (for water). PMMA latexes in alkanes were diluted to a volume fraction ($\phi$) of $10^{-3}$ into a solution of AOT at a concentration of 100 mM. Silica dispersions in water were diluted to an acceptable turbidity. For nonpolar solvents, the applied field strength was $2.0 \times 10^4$ V m$^{-1}$, and six runs of 50 measurements were averaged. For water, the applied field strength was $2.5 \times 10^4$ V m$^{-1}$, and five runs of variable numbers of measurements were averaged.

## 3. Results and discussion

As mentioned in Section 1, three systems of colloids in nonpolar solvents (water-in-oil microemulsions, surfactant-stabilized silica organosols, and sterically-stabilized PMMA latexes) are compared. All contain polar components which on their own are immiscible with alkanes, and these are sterically stabilized using a hydrocarbon chain. All have AOT surfactant added.

Water-in-oil microemulsions are thermodynamically stable dispersions with very small droplet sizes (typically < 100 Å) [19]. The amount of dispersed water is quantified by the $w$ ratio, equal to [water]/[AOT].

Silica organosols consist of surfactant-coated nanoparticles which have been transferred into organic solvent [15,24]. Different surfactants have been used to disperse silica nanoparticles, depending on the nature of the solvent and the particle surface chemistry [15]. Several groups have recently studied charges of silica nanoparticles dispersed in alkanes in the presence of AOT [37–41], but only very small concentrations of silica can be dispersed due to the lack of Coulombic attraction between AOT anions and the negatively charged silica surfaces. Alumina nanoparticles can also be charged in alkanes in the presence of AOT [40]. However, these studies are generally performed at low particle concentrations, but by using the method of Tabor et al., highly concentrated dispersions can be prepared, promoted by the Coulombic attraction between AOT and the alumina-modified 30CAL25 surface [15].

The chemistry to produce sterically-stabilized PMMA latexes has been well-established, primarily using a steric stabilizer brush copolymer of PHSA [21,42]. The stabilizer brush copolymer consists of a methacrylate-tipped PHSA, methyl methacrylate, and glycidyl methacrylate [29]. This synthetic approach achieves latexes with low dispersity that are stable in aliphatic solvents.

In this section, two properties of these nonaqueous colloids will be discussed with the goal of determining the distribution, partitioning, and localization of added AOT surfactant. The stability of the colloids in different solvents will be discussed first. SANS measurements of the colloids with both core and AOT contrasts will then be discussed. This discussion will consist partly of new data and partly of reinterpretations of data in the literature [16,22,36] to give a comprehensive view on the distribution of AOT in different systems.

### 3.1. Varying solvent and effect on stability

#### 3.1.1. Water-in-oil microemulsions

The effects of varying the alkane on the phase stability and scattering of water-in-oil microemulsions have been discussed extensively by Robinson et al. [22,23]. As the chain-length of the alkane solvent is increased (for example, from heptane to dodecane), less water can be solubilized in the microemulsions, and the maximum $w$ value that can be stabilized decreases across the accessible temperature range. $w$–$T$ phase diagrams for these three oils are shown in Fig. 2. SANS measurements of $w = 20$ microemulsions in these solvents support the data in Fig. 2; in heptane and decane, the microemulsion droplets are similar, and in dodecane, the microemulsion droplets are large with high dispersity. (SANS curves and fits to spherical form factors are shown in Supporting Material, Fig. S1 and Table S1.)

Several explanations have been proposed as the origin of the differing stability of surfactant-stabilized water–oil films. The phase behavior can be normalized by a parameter such as either the critical temperature [23] or the density of the alkane under increased pressure [43,44]. This suggests that it is the physical properties of the alkanes under specified conditions that causes solvent effects. An alternative explanation is that the bending elasticity constant of the AOT layer at the oil–water interface varies in different alkanes, causing the extent of oil penetration to vary as well [45]. Regardless of the exact origin of the solvent effects, it is clear from the literature (demonstrated well in Fig. 2) that there is a difference in microemulsion stability with varying chain length of the alkane solvent. This is consistent with AOT being located at the water–oil interface.

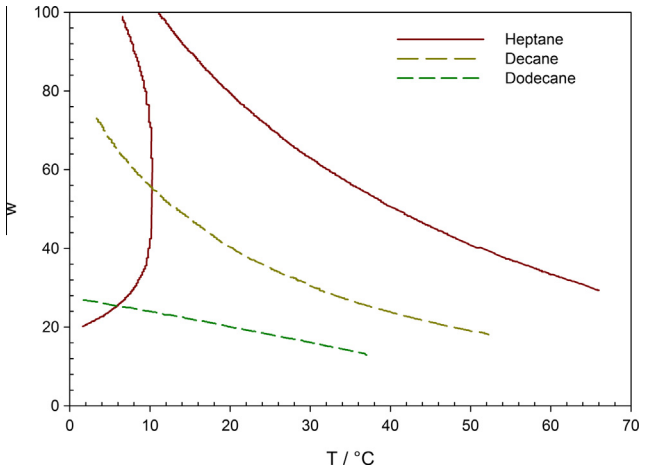


**Fig. 2.** Phase behavior of water-in-oil microemulsions in heptane, decane, and dodecane at an AOT concentration of 100 mM. The area under the curve represents the microemulsion phase; above this curve, there are two phases present. (Data are reproduced from Robinson et al. [22].)

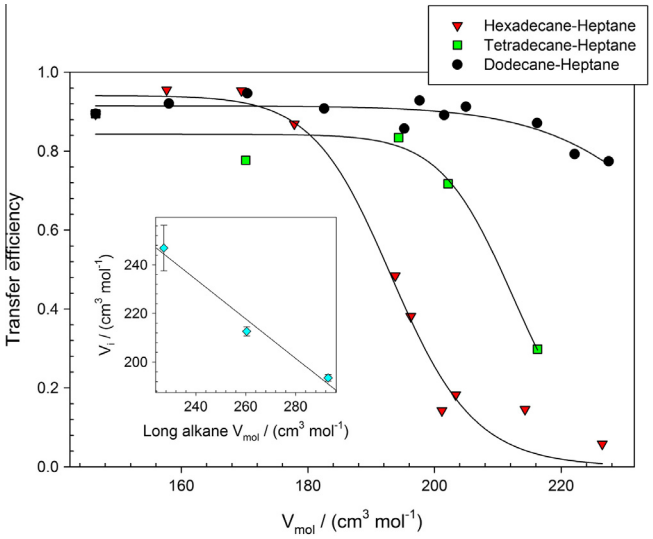


**Fig. 3.** The transfer efficiency ($E$) of silica organosols as a function of $V_{mol}$ for samples with 2 wt.% 30CAL25 silica and 4 wt.% AOT. Longer-chain alkanes lead to dispersion instability at lower $V_{mol}$ than shorter-chain alkanes, demonstrating a tangible effect of varying solvent on dispersions. The curves are fits to Eq. (2). The subfigure shows $V_i$ as a function of the longer-chain alkane $V_{mol}$. This quantifies the difference in stability between the different alkane mixtures.

### 3.1.2. Surfactant-stabilized silica organosols

In the first report of such surfactant-stabilized silica organosols, the dispersions were found to be stable in several solvents (cyclohexane, toluene, and heptane) as well as their mixtures [15]. In longer chain alkanes, the dispersions are found to become unstable [24]. This latter study, however, was limited by only considering two binary solvent systems. The solvent pairs were normalized by the effective molecular volume ($V_{mol}$) assuming ideal mixing, calculated by summing the mol fraction-weighted molecular volumes of the solvents alone. In reality, there is a small excess molar volume that arises from mixing alkane solvents. The excess molar volumes for the binary solvents used in this study are negative and less than 1 $cm^3\ mol^{-1}$ [46,47]. The magnitude of this nonideality is small compared to the magnitude of $V_{mol}$ ($\sim 100\ cm^3\ mol^{-1}$), and any differences are within the error of data fitting. Therefore, it is appropriate to use $V_{mol}$ calculated assuming ideal mixing.

By restricting this study to alkane solvents, which have similar intermolecular interactions, it is possible to isolate the influence of the solvent $V_{mol}$ on the stability of the dispersion. Three long-chain alkanes have been selected (dodecane, tetradecane, and hexadecane) and have been prepared in mixtures with heptane to give $V_{mol}$ values spanning that of pure heptane ($146\ cm^3\ mol^{-1}$) to that of pure dodecane ($228\ cm^3\ mol^{-1}$). The transfer efficiency ($E$), the fraction of silica remaining dispersed after gentle centrifugation, is measured for each dispersion. The results of these measurements are shown in Fig. 3. As $V_{mol}$ of heptane–alkane mixtures cannot be less than that of heptane, $V_0$ is defined as $V_{mol}$ of heptane.

To quantify the relationship between dispersion stability and alkane size, the data in Fig. 3 can be fit to a logistic function, which is appropriate given the asymptotic limits at extreme values of $V_{mol}$. Eq. (2) has been used to fit the data. The transfer efficiency ($E(V_{mol})$) is a function of the limiting transfer efficiency ($\lim_{V_{mol}\to 0} E(V_{mol}) = E_0$), the molar volume at the inflection point ($V_i$), and the exponent $n$, which relates to the steepness of the transition between the two asymptotes. At $\lim_{V_{mol}\to\infty}$, the transfer efficiency decreases to 0.

$$E(V_{mol} - V_0) = \frac{E_0}{1 + \left(\frac{V_{mol}-V_0}{V_i-V_0}\right)^n} \tag{2}$$

As can be seen in Fig. 3, the logistic function gives a very good fit to the data. At $V_{mol} = V_0$, the fit values of $E_0$ are all similar ($E_0 \approx 0.9$). The inflection point of the function in the different solvent mixtures, however, is very different, and the fit values of $V_i$ as a function of long-chain alkane $V_{mol}$ are shown in the inset of Fig. 3. (The values of the fits are shown in Supporting Material, Table S2.) The relationship between $V_i$ and the long-chain alkane $V_{mol}$ is linear, and this demonstrates a strong correlation between the two. (The error for $V_i$ in dodecane–heptane mixtures is large because $V_i$ is greater than $V_{mol}$ for pure dodecane so cannot be reached.)

The data in Fig. 3 clearly shows the effect of varying the solvent type on the stability of the silica dispersions. The different solvent mixtures are prepared to have the same $V_{mol}$, rather than at the same mol fraction, and therefore, it is even more remarkable that the longer alkanes destabilize the dispersions at lower $V_{mol}$. The results for the dodecane–heptane mixtures differ from the literature [24], where complete instability was observed in pure dodecane. However, the particle sizes used in the two studies are different ($r = 15$ nm for 30CAL25 and $r = 38$ nm for 30CAL50), which clearly has an effect.

In addition to observing the bulk stability of the organosols, SANS measurements have been performed on the dispersions to determine if there are any significant structural differences as a consequence of varying solvent. The scattering length density ($\rho$) of the solvent was matched to the silica cores to isolate the scattering from the AOT surfactant. (The value of $\rho$ for the silica is $3.64 \times 10^{-6}$ Å$^{-2}$, measured experimentally from the scattering in different $H_2O/D_2O$ mixtures, shown in Supporting Material, Fig. S2. This agrees well with the literature [48].).

SANS data from 30CAL25 organosols in dodecane and heptane are shown in Fig. 4. The data have been modeled as a linear summation of contributions from AOT inverse micelles and from AOT on the silica particle surfaces, which has previously been shown to be appropriate for these systems [15]. (Only the summed curves are shown in Fig. 4. The individual curves are shown in Supporting Material, Fig. S3. The best fit values to the SANS data are also shown in Supporting Material, Tables S3 and S4.) This model gives a good fit to the data, although there are some deviations at low-$Q$ and at the first fringe at mid-$Q$. This can be ascribed to a combination of particle inhomogeneities and residual scattering from the particle cores.

The curves in heptane and dodecane are very similar, particularly at high-$Q$, corresponding to the AOT inverse micelles.

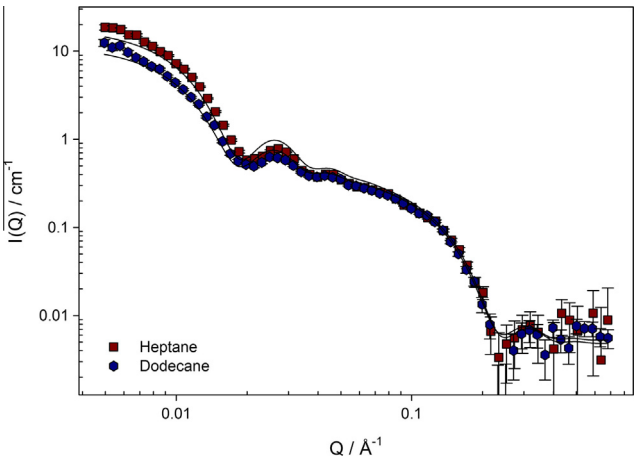


**Fig. 4.** SANS of AOT-stabilized silica organosols with 2 wt.% 30CAL25 and 4 wt.% AOT in heptane and dodecane core-matched solvent. The measured data are well described by a summation of contributions from AOT inverse micelles and an AOT shell around the silica particles. There is little difference in the inverse micelles in the two solvents at high-*Q*, and there is a small difference in the thickness of the shell and the contrast ($\Delta\rho$) between the shell and core in the scattering from the AOT shell at low-*Q*. (Fit parameters are shown in Supporting Material, Tables S3 and S4.)

At low-*Q*, the profiles of the curves are similar but the intensities differ slightly. This is due predominantly to a difference in the fit values of $\Delta\rho$ between core and shell ($\Delta\rho$ in heptane = $2.6 \times 10^{-6}$ Å$^{-2}$ and $\Delta\rho$ in dodecane = $1.9 \times 10^{-6}$ Å$^{-2}$), which indicates that there is more surfactant on the surfaces of the organosols in heptane. Additionally, there is a slight difference in the thickness of the shell ($t$ in heptane = 28 Å and $t$ in dodecane = 30 Å), although the difference in $\Delta\rho$ is the more significant parameter. SANS measurements have also been performed for silica organosols dispersed in binary alkane solvents (hexadecane–heptane and dodecane–heptane) at solvent $V_{mol}$ = 171 and 182 cm$^3$ mol$^{-1}$ where the organosols are still highly stable (Fig. 3). These data are shown in Supporting Material (SANS curves in Fig. S4 and model fits in Tables S3 and S4). The profiles and intensity of these curves are very similar regardless of the solvent mixture, but the trends in the model fits are similar to those in pure heptane and dodecane. Organosols in hexadecane–heptane mixtures, which include a higher proportion of heptane at a specified $V_{mol}$, have thinner and more concentrated AOT layers ($t \approx 24$ Å and $\Delta\rho \approx 2.3 \times 10^{-6}$ Å$^{-2}$, average of both compositions) than in dodecane–heptane mixtures, which include a lower proportion of heptane ($t \approx 34$ Å and $\Delta\rho \approx 1.6 \times 10^{-6}$ Å$^{-2}$, average of both compositions). Also, in order to ensure that differences in the AOT inverse micelles themselves were not responsible for this difference in stability, SANS measurements of AOT in mixtures of heptane-$d_{16}$ with hexadecane, tetradecane, and dodecane were performed. These data are shown in Supporting Material (SANS curves in Fig. S5 and model fits in Table S5). No differences in the structure of the AOT inverse micelles is observed.

The fact that varying the solvent has an effect on the stability of the silica dispersions and the thickness and density of the AOT layer suggests that the AOT is located at the silica-oil interface. This is also the case for microemulsions, although the origin of the solvent-induced instability for silica dispersions may be different to microemulsions, given that curves cannot be normalized by using a parameter such as the solvent $V_{mol}$.

### 3.1.3. Sterically-stabilized PMMA latexes

Two properties of the PMMA latexes will be considered: stability and electrophoretic mobility in different alkane solvents. The latexes are studied both with and without added AOT. The specific particles in this study are stabilized by a poly(12-hydroxystearic acid) PHSA brush copolymer [21], and AOT has been frequently used as a charge control agent for such particles [16,27,28,49].

The stability of the latexes in alkane solvents has been observed for 24 h, and images at the start and finish are shown in Fig. 5. The dispersions have been prepared in both pure solvent (Fig. 5a and c) and with 100 mM AOT added (Fig. 5b and d). The identity of the solvent does not appear to considerably change the stability of the dispersions. Some sedimentation is observed in the solvents, particularly octane, but this is due to a density mismatch between PMMA and solvent, not a solvent-induced instability. The average density of PMMA latexes is 1.09 g cm$^{-3}$ [50], and the densities of the alkanes are 0.70 g cm$^{-3}$ for octane, 0.75 g cm$^{-3}$ for dodecane, and 0.77 g cm$^{-3}$ for hexadecane [51]. Solvent-induced instability would lead to sedimentation of nearly all the particles, as was the case for the silica organosols (Fig. 3). This appears to be a function of the stabilizer polymer that is used. The latexes in this study are stabilized by PHSA and are stable from octane to hexadecane, but latexes stabilized by poly(dimethylsiloxane) are only stable up to dodecane and not in hexadecane [52].

In addition to the stability of the particles, the electrophoretic mobility of latexes with AOT added has been measured. The electrophoretic mobility ($\mu$) is the constant of proportionality between the velocity ($\vec{v}$) of a charged particle and the electric field ($\vec{E}$), shown in Eq. (3) [53].

$$\vec{v} = \mu\vec{E} \tag{3}$$

The electrophoretic mobility of a charged particle in a solvent depends on the properties of the fluid, specifically the viscosity ($\eta$) and the relative permittivity of the medium ($\epsilon_r$). The permittivity is conveniently accounted for by considering the Bjerrum length ($\lambda_B$) of the solvent, shown in Eq. (4), the length where the Coulombic attraction is equal to the thermal energy ($k_BT$) [54]. It depends on the elementary charge ($e$), the vacuum permittivity ($\epsilon_0$), and $\epsilon_r$.

$$\lambda_B = \frac{e^2}{4\pi\epsilon_0\epsilon_r k_B T} \tag{4}$$

Equivalently charged particles will move more slowly in a higher viscosity fluid and more rapidly in a lower permittivity fluid. To normalize for this, a scale for the electrophoretic mobility ($\mu_0$) can be defined, shown in Eq. (5), equal to the mobility of a sphere of charge $e$ with a radius equal to $\lambda_B$ in a solution with viscosity $\eta$ [55].

$$\mu_0 = \frac{e}{6\pi\eta\lambda_B} \tag{5}$$

Both the experimental mobilities ($\mu$) and the reduced mobilities ($\mu/\mu_0$) for PMMA latexes in 100 mM AOT solutions are shown in Table 1. The values of $\mu$ vary over an order of magnitude between octane and hexadecane, but this is a consequence of the increase in viscosity ($\eta = 0.51$ mPa s for octane, $\eta = 3.0$ mPa s for hexadecane [56]). The consequence of this can clearly seen by comparing the values of $\mu/\mu_0$ for octane, dodecane, and hexadecane, which are equal within the error.

The fact that PMMA latexes are stable and equivalently charged in the presence of AOT in different alkanes indicates that the AOT does not seem to be important in determining the stability and properties of the latexes. The identity of the stabilizer polymer seems to have more of an influence, as, for example, PHSA-stabilized latexes are stable in hexadecane [28,57–60] whereas PDMS-stabilized latexes are not [52].

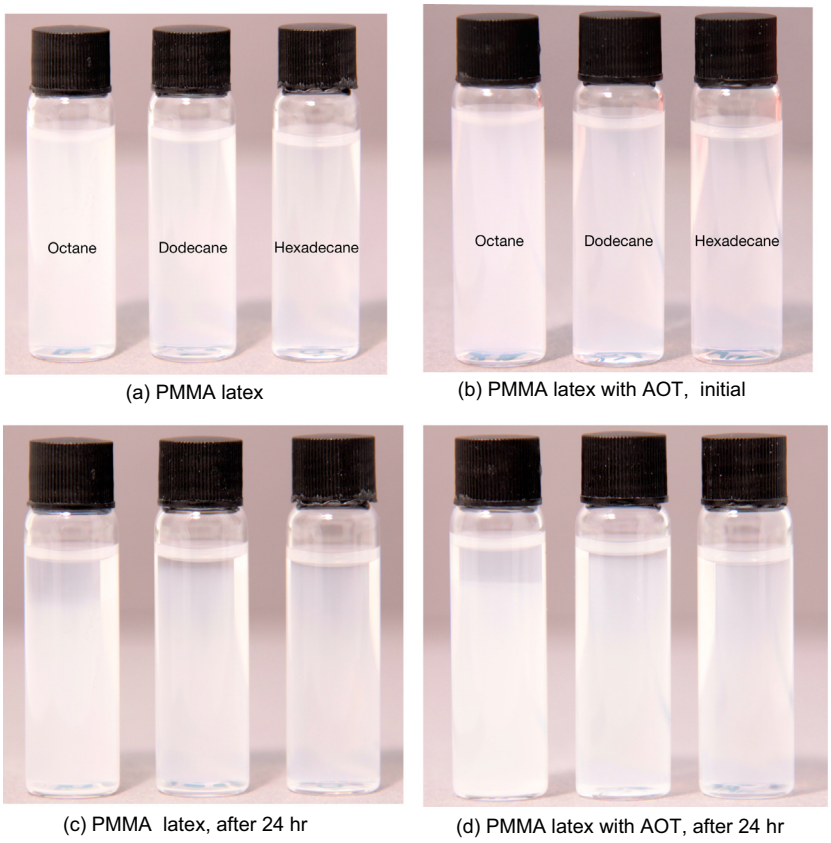


**Fig. 5.** Photographs of PMMA latexes in three alkanes of different chain lengths (octane, dodecane, and hexadecane) both with and without added AOT to monitor sedimentation over 24 h. The small amount of sedimentation is due to the density mismatch between PMMA latexes and the alkanes, rather than solvent-induced destabilization. The addition of surfactant does not cause any visible change.

**Table 1**
Electrophoretic mobilities of PMMA latexes in alkanes with [AOT] = 100 mM.

| Solvent | $\mu/(10^{-9}\ m^2\ V^{-1}\ s^{-1})$ | $\mu/\mu_0$ |
|---|---|---|
| Octane | $-2.0 \pm 0.3$ | $-3.8 \pm 0.6$ |
| Dodecane | $-0.8 \pm 0.1$ | $-3.9 \pm 0.6$ |
| Hexadecane | $-0.38 \pm 0.07$ | $-4.1 \pm 0.8$ |

### 3.2. Structure of AOT layers by SANS

The structures of the AOT layers in these three colloidal systems have also been studied using SANS by considering two contrasts. Scattering from colloid cores is highlighted by performing measurements on stable colloids. For water-in-oil microemulsions, $D_2O$ is added with AOT in unlabeled heptane. For silica colloids, dispersions are prepared in $H_2O$ where the particles are stable. For PMMA latexes, dispersions are prepared in unlabeled dodecane. Scattering from AOT is highlighted by matching the alkane solvent to the core and using appropriately labeled AOT.

Some SANS results have been presented earlier in this paper (Fig. 4 and in Supporting Material). In this section, scattering measurements will be generalized and used to study the differences and similarities of the structures in the systems, rather than modeling the data. The particles are of a different size and composition, so the $Q$-range that the particles scatter over as well as the intensity of scattering will be different for each. This makes normalization necessary; natural scales can be developed to normalize the scattering curves for systems on different scales.

The scattered intensity per unit volume is given in Eq. (6) [61]. It is a function of the volume fraction ($\phi$), the volume of the particle ($V_p$), the contrast between particle and solvent ($\Delta\rho$), and the form factor $P(Q)$, which depends on the particle geometry. No structure factor ($S(Q)$) is required to fit the data due to low interparticle interactions in low dielectric solvents, and so it can be excluded.

$$I(Q) = \phi V_p \Delta\rho^2 P(Q) S(Q) \tag{6}$$

To normalize the intensity ($I(Q)$ axis), the Guinier approximation, shown in Eq. (7) [61], is used to determine the SANS intensity at $Q = 0$ (referred to as $I(Q = 0)$). The Guinier approximation also gives the radius of gyration ($R_g$) of the scattering particles. $I(Q = 0)$ and $R_g$ can be obtained from a plot of $\ln I(Q)$ as a function of $Q^2$.

$$\ln I(Q) = -\ln I(Q = 0) \cdot \frac{(QR_g)^2}{3} \tag{7}$$

Using this value of $I(Q = 0)$, all SANS curves were normalized to give an intensity independent scattering curve. This effectively reduces the scattering curves to the form factor ($P(Q)$) without any *a priori* information about the composition of the particles.

To normalize the $Q$ axis, the difference in particle size needs to be accounted for. $\vec{Q}$ is the scattering or momentum transfer vector defined as the difference between the incident and scattered wave vectors ($\vec{Q} = \vec{k_s} - \vec{k_i}$). The magnitude of $\vec{Q}$ is defined in Eq. (1), and by using the Bragg law, the expression shown in Eq. (8) can also be used to define the magnitude of $Q$ [61]. This relates the magnitude of $Q$ to the lengthscale being measured ($d$).

$$Q = \frac{2\pi}{d} \tag{8}$$

This provides a simple way to normalize the $Q$-axis for particles of different sizes. By rearranging Eq. (8) and substituting the particle radius for the lengthscale ($2r = d$), a size independent

**Table 2**
Core radii $r$ for particles from SANS data.

| Particle system | $r$/Å | $\sigma$ |
|---|---|---|
| $D_2O$-in-heptane microemulsions, $w = 30$[a] | 46 | 0.22 |
| CAL25 dispersions in $H_2O$ | 147 | 0.14 |
| PMMA latexes in dodecane[b] | 335 | 0.20 |

Published particle sizes: [a] Nave et al. [36] and [b] Smith et al. [16].

scattering curve can be obtained by plotting $Qr/\pi$ as the $x$-axis. The values of $r$ have either been fit in this study or are taken from the literature and are shown in Table 2, along with the values of the Schulz dispersity ($\sigma$) [62].

### 3.2.1. Particle core scattering

SANS measurements of colloid cores will be discussed first to confirm the applicability of the normalization procedure discussed in the previous section. Core contrast for SANS consists of $D_2O$-in-heptane microemulsions, 30CAL25 dispersions in $H_2O$, and PMMA latexes in dodecane. (The SANS data for PMMA latexes were previously published [16].) The normalized scattering curves are shown in Fig. 6.

The normalized scattering intensity ($I(Q)/I(Q=0)$) approaches 1 at low-$Q$, although the difference in particle sizes means that the larger colloids (silica particles and PMMA latexes) do not reach a sufficiently low-$Q$ to reach an asymptote. Guinier-type plots of the normalized SANS data (Supporting Material, Fig. S6 and Table S6) are essentially equivalent, and as expected, the values of $I(Q)/I(Q=0) \approx 1$. The normalized $Q$-axis ($(Qr)/\pi$) dependence of the scattering also agrees for the three colloids. The 30CAL25 particles deviate slightly from the other two colloids, and this is likely due to hydration leading to poorly defined particle interfaces for silica in water. The curves are plotted on a semi-log axis to emphasize the similarities at low-$Q$, but all the curves show the expected scattering from spheres in the high-$Q$ Porod region. Log–log plots of this normalized SANS data are shown in Supporting Material, Fig. S7.

From the data in Fig. 6 and Guinier-type plots of the normalized SANS data, it is clear that the normalization procedure is appropriate for reducing the scattering curves to a single master curve. This shows that the cores of the colloids on normalized axes can be considered to be equivalent.

### 3.2.2. AOT scattering

Having established that the normalization approach is appropriate for small-angle scattering data, the same procedure is performed for SANS measurements where the AOT component is highlighted. AOT contrast consists of $D_2O$-in-heptane-$d_{16}$ microemulsions, AOT-stabilized 30CAL25 organosols in silica contrast matched heptane, and AOT-$d_{34}$ with PMMA latexes in PMMA contrast matched dodecane. (The data from the $D_2O$-in-heptane-$d_{16}$ microemulsions [36] and the AOT-$d_{34}$ with PMMA latexes [16] were previously published.) The same $r$ (Table 2) as for the core SANS normalization is used for the $Q$-axis normalization. If the AOT is adsorbed, the curves should shift to lower-$Q$ (larger size), whereas if the AOT is absorbed, then the curve should be the same as for the cores alone.

Fig. 7 shows the normalized SANS curves for AOT-highlighted samples. It is clear that the curves are no longer equivalent, as was the case for the core scattering in Fig. 6. This provides strong evidence that the added AOT surfactant has a different distribution in the three systems.

It is worth noting several further points about the SANS curves. The curves are plotted on a semi-log axis to emphasize the similarities at low-$Q$, but core–shell form factors show pronounced peaks

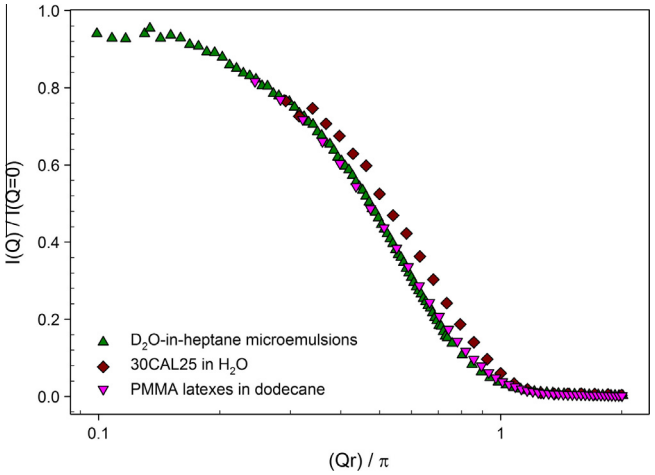


**Fig. 6.** Normalized SANS of colloid cores ($D_2O$-in-heptane microemulsions, 30CAL25 dispersions in $H_2O$, and PMMA latexes in dodecane). By normalizing the SANS data, the curves fall onto a single curve. This confirms that normalizing by $I(Q=0)$ and $r$ is valid.

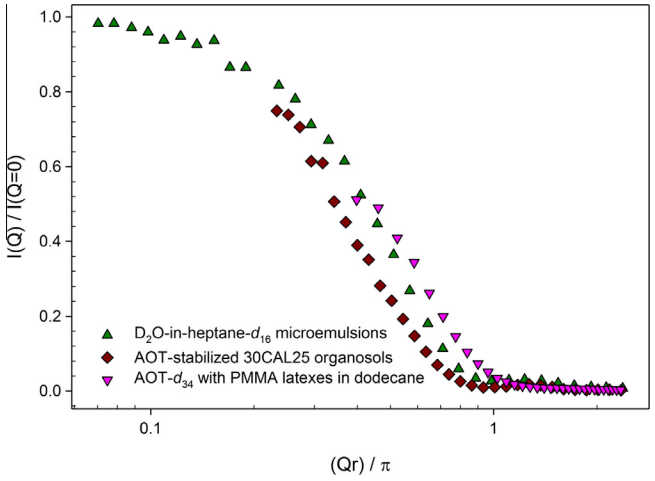


**Fig. 7.** Normalized SANS of nonaqueous colloids with AOT highlighted ($D_2O$-in-heptane-$d_{16}$ microemulsions, AOT-stabilized 30CAL25 organosols in silica contrast matched heptane, and AOT-$d_{34}$ with PMMA latexes in PMMA contrast matched dodecane). The curves do not fall onto a single curve, indicating that the structure of the AOT layer is not equivalent.

at high-$Q$ arising from the layer thickness. These peaks are not visible on a semi-log plot, but the peaks are visible on log–log plots, which are shown in Supporting Material, Fig. S8. Also, there does not seem to be any effect of solvent on the AOT-highlighted normalized scattering, as the 30CAL25 organosols in heptane and dodecane give the same scattering curves. This is shown in Supporting Material, Fig. S9. Finally, for both AOT-stabilized 30CAL25 organosols and AOT-$d_{34}$ with PMMA latexes, there are free AOT inverse micelles in solution. The scattering from free AOT has been subtracted from these scattering curves, in accordance with literature [15,16,49].

To truly assess how the colloid cores and the added AOT differ structurally, it is worthwhile comparing the two normalized SANS curves for each system. This comparison is shown in Fig. 8. The differences between the three systems are immediately apparent. The core and AOT-highlighted scattering from the microemulsions (Fig. 8a) and silica organosols (Fig. 8b) are very different, with the AOT-highlighted scattering shifting to lower-$Q$. This indicates that the whole scattering center is larger than the radius of the

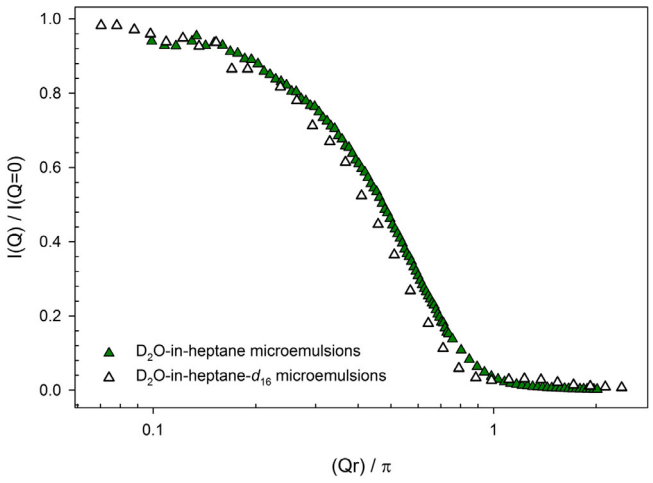


(a) $D_2O$-in-heptane microemulsions

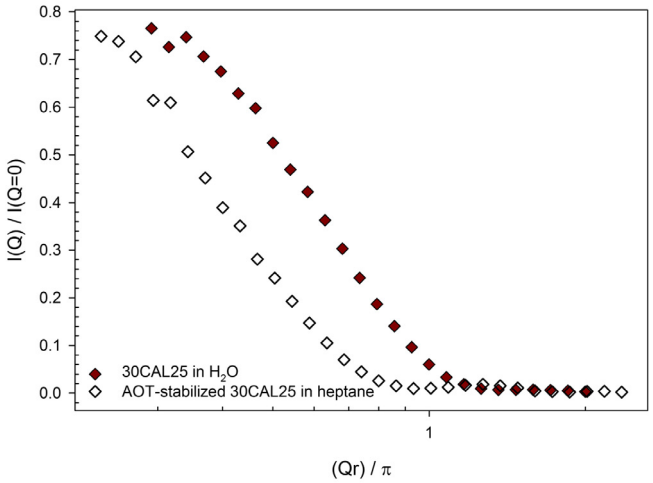


(b) 30CAL25 organosols

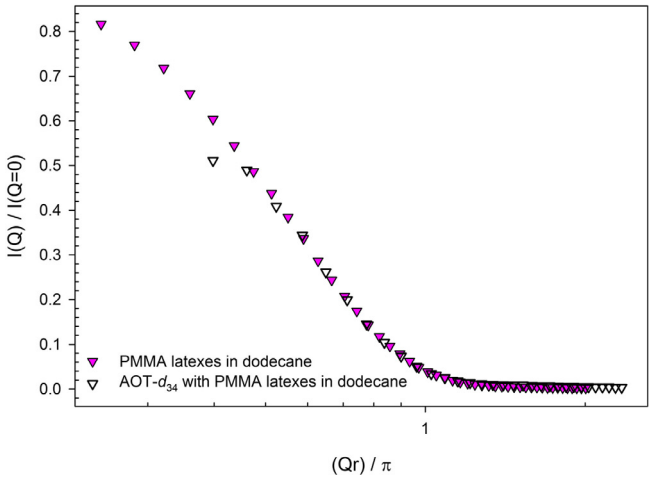


(c) PMMA latexes

**Fig. 8.** Normalized SANS of core vs. AOT-highlighted scattering for systems of nonaqueous colloids. The two curves for $D_2O$-in-heptane microemulsions and for 30CAL25 organosols are different, whereas the two curves for the PMMA latexes are essentially identical.

particle. The difference in the amount that the scattering is shifted is due to the ratio of the shell thicknesses to the core radii. The curves from the core and AOT-highlighted scattering for the PMMA latexes in dodecane (Fig. 8c), however, are essentially identical. This indicates that for this system the structure of the PMMA cores and the space that the AOT fills are the same.

### 3.3. Adsorption or absorption?

In the previous sections, two studies of model nonaqueous colloids have been considered: the effects of solvent variation and the distribution of the surfactant AOT as measured by SANS. These have helped provide insight into the colloids and the way that AOT, as a typical example surfactant, interacts with different systems. Referring back to Fig. 1, this interaction of the surfactant with the colloids can be considered as two extremes, adsorption or absorption. It appears that the exact interaction of AOT with nonaqueous colloids depends on the specific system under study.

As expected, AOT in water-in-oil microemulsions and surfactant-stabilized silica organosols adsorbs at the particle surfaces. Varying solvent has a profound effect on the stability of the colloids, due to the AOT molecules being located at the colloid surfaces where changes in adsorbate–solvent interactions lead to destabilization in longer-chain alkanes. Normalized SANS measurements also show marked differences between scattering comparing the particle cores and added AOT. These analyses are consistent with AOT shells coating the polar cores.

On the other hand, AOT absorbs into the PHSA-stabilized PMMA latex cores. There is no effect of varying solvent on either the stability of the colloids or their electrophoretic mobility. The latexes are equally stable with and without added AOT, demonstrating that it is the brush copolymer mediating the colloid-solvent interactions. Normalized SANS measurements show no difference between scattering from the particle cores and from the added AOT, demonstrating that the contrasted species in both fills the same volume. This was proposed recently in a detailed contrast-variation SANS study of this system [16], but more certainty has been obtained by considering the PMMA latexes in context with other model nonaqueous colloids.

The systems are not entirely this simple, as AOT is also present as monomers in both organic solvents and water, in addition to forming interfacial layers, inverse micelles, and absorbed surfactants. Strictly some AOT must be dissolved (alternatively "absorbed") into the water cores of microemulsions, but it will only be present at the level of the critical micelle concentration in water (2.56 mM [63]). Likewise, some AOT is dissolved into the organic solvent at the level of the critical micelle concentration in oil (0.12 mM in cyclohexane, for example [64]). These concentrations are much less than the concentrations of AOT used ($\sim$ 100 mM), so the majority of AOT is present either at interfaces or as inverse micelles.

Why does AOT adsorb onto some colloids and absorb into others? Clearly, the details of the system are important. For silica organosols, it is obvious that AOT can only adsorb; these are solid nanoparticles, unlikely to be penetrated by organic species. For microemulsions and PMMA latexes, it is worthwhile considering the colloid interiors as a "solvent." The cores of sterically-stabilized PMMA latexes can be penetrated by small molecules [65–67], which shows that it is reasonable to consider the cores as a "solvent." The Hildebrand solubility parameter ($\delta$, the cohesive density) can be used as an index to determine the solubility of a species; similar cohesive densities have a higher affinity to dissolution. The value of $\delta$ for AOT is 25.0 $MPa^{1/2}$, for PMMA is 19.0 $MPa^{1/2}$, and for water is 47.9 $MPa^{1/2}$ [68]. While AOT is soluble and acts as a surfactant in water [63], given these values of $\delta$, it is more likely in nonpolar solvents that AOT would be "dissolved" in PMMA than in water.

## 4. Conclusions

Colloids in nonpolar solvents are used extensively in industry [1–12], and in addition to their many applications, they provide excellent model systems, in some cases even behaving effectively as hard spheres [18]. Although their physical interactions are simple, their chemical compositions can be complex, requiring the addition of surfactant molecules to either stabilize the polar cores or to impart charge. Three ternary systems of nonaqueous colloids have been considered in this study, consisting of a polar core, a nonpolar solvent, and added surfactant. The nature of the added surfactant is of primary importance to the stability and activity of the colloids, and the distribution of this component has been studied. As an amphiphilic molecule, the surfactant AOT can be distributed either in water [63] or oil [36]. The distribution of AOT in these ternary systems can be considered as two limiting cases: adsorption, where it is located preferentially at the interface, or absorption, where it is located throughout the colloids. Whether adsorption or absorption occurs depends on the chemical nature of the colloid cores. Water and silica do not allow extensive penetration of AOT; therefore, adsorption dominates for water-in-oil microemulsions and surfactant-stabilized silica organosols. PMMA latexes are sufficiently porous [65–67] to allow penetration of AOT; therefore, absorption can occur for PMMA latexes. It is not sufficient to assume that surfactants behave as their name implies and act as only as "surface-active agents" [69] at colloidal surfaces. By considering ternary systems, there can be multiple interfaces, both on the interior and exterior of the colloids. The experiments presented here act as a template for future studies on the structures present in colloidal systems as a function of both surfactant and colloid type.

## Acknowledgments

GNS acknowledges Merck Chemicals Ltd. UK, an affiliate of Merck KGaA, Darmstadt, Germany, and the UK Engineering and Physical Sciences Research Council (EPSRC) for the provision of a CASE PhD studentship. The authors thank the UK Science and Technology Facilities Council (STFC) for allocation of beamtime at ISIS and the ILL and grants toward consumables and travel. This work benefitted from SasView software, originally developed by the DANSE Project under NSF award DMR-0520547.

## Appendix A. Supplementary material

Supplementary data associated with this article can be found, in the online version, at http://dx.doi.org/10.1016/j.jcis.2014.12.048.

## References

[1] J. Eastoe, M.J. Hollamby, L. Hudson, Adv. Colloid Interface Sci. 128–130 (2006) 5–15, http://dx.doi.org/10.1016/j.cis.2006.11.009.
[2] J. Galsworthy, S. Hammond, D. Hone, Curr. Opin. Colloid Interface Sci. 5 (5–6) (2000) 274–279, http://dx.doi.org/10.1016/S1359-0294(00)00066-2.
[3] L. Hudson, J. Eastoe, P. Dowding, Adv. Colloid Interface Sci. 123–126 (2006) 425–431, http://dx.doi.org/10.1016/j.cis.2006.05.003.
[4] M.E. Leunissen, C.G. Christova, A.-P. Hynninen, C.P. Royall, A.I. Campbell, A. Imhof, M. Dijkstra, R. van Roij, A. van Blaaderen, Nature 437 (7056) (2005) 235–240, http://dx.doi.org/10.1038/nature03946.
[5] P. Bartlett, A.I. Campbell, Phys. Rev. Lett. 95 (12) (2005) 128302, http://dx.doi.org/10.1103/PhysRevLett.95.128302.
[6] I.D. Morrison, Colloids Surf. A: Physicochem. Eng. Aspects 71 (1) (1993) 1–37, http://dx.doi.org/10.1016/0927-7757(93)80026-B.
[7] G.N. Smith, J. Eastoe, Phys. Chem. Chem. Phys. 15 (2) (2013) 424–439, http://dx.doi.org/10.1039/c2cp42625k.
[8] A. Klinkenberg, J.L. van der Minne (Eds.), Electrostatics in the Petroleum Industry: The Prevention of Explosion Hazards, Elsevier, London, 1958.
[9] B. Comiskey, J.D. Albert, H. Yoshizawa, J. Jacobson, Nature 394 (6690) (1998) 253–255, http://dx.doi.org/10.1038/28349.
[10] Y. Chen, J. Au, P. Kazlas, A. Ritenour, H. Gates, M. McCreary, Nature 423 (6936) (2003) 136, http://dx.doi.org/10.1038/423136a.
[11] J. Heikenfeld, P. Drzaic, J.-S. Yeo, T. Koch, J. Soc. Info. Display 19 (2) (2011) 129–156, http://dx.doi.org/10.1889/JSID19.2.129.
[12] V. Novotny, Colloids Surf. 24 (4) (1987) 361–375, http://dx.doi.org/10.1016/0166-6622(87)80241-X.
[13] C. Wohlfarth, in: CRC Handbook of Chemistry and Physics, 92nd ed., CRC Press, 2012.
[14] J. Eastoe, B.H. Robinson, D.C. Steytler, D. Thorn-Leeson, Adv. Colloid Interface Sci. 36 (1991) 1–31, http://dx.doi.org/10.1016/0001-8686(91)80027-H.
[15] R.F. Tabor, J. Eastoe, P.J. Dowding, I. Grillo, R.K. Heenan, M. Hollamby, Langmuir 24 (22) (2008) 12793–12797, http://dx.doi.org/10.1021/la802486k.
[16] G.N. Smith, S. Alexander, P. Brown, D.A.J. Gillespie, I. Grillo, R.K. Heenan, C. James, R. Kemp, S.E. Rogers, J. Eastoe, Langmuir 30 (12) (2014) 3422–3431, http://dx.doi.org/10.1021/la500331u.
[17] M. Kotlarchyk, S.-H. Chen, J.S. Huang, M.W. Kim, Phys. Rev. A 29 (4) (1984) 2054–2069, http://dx.doi.org/10.1103/PhysRevA.29.2054.
[18] P.N. Pusey, W. van Megen, Nature 320 (6060) (1986) 340–342, http://dx.doi.org/10.1038/320340a0.
[19] D. Langevin, Acc. Chem. Res. 21 (7) (1988) 255–260, http://dx.doi.org/10.1021/ar00151a001.
[20] W. Ostwald, Kolloid Z. 45 (4) (1928) 331–345, http://dx.doi.org/10.1007/BF01423432.
[21] L. Antl, J. Goodwin, R. Hill, R. Ottewill, S. Owens, S. Papworth, J. Waters, Colloid. Surface. 17 (1) (1986) 67–78, http://dx.doi.org/10.1016/0166-6622(86)80187-1.
[22] B.H. Robinson, C. Toprakcioglu, J.C. Dore, P. Chieux, J. Chem. Soc., Faraday Trans. 1 80 (1) (1984) 13–27, http://dx.doi.org/10.1039/F19848000013.
[23] C. Toprakcioglu, J.C. Dore, B.H. Robinson, A. Howe, P. Chieux, J. Chem. Soc., Faraday Trans. 1 80 (2) (1984) 413–422, http://dx.doi.org/10.1039/F19848000413.
[24] A. Salabat, J. Eastoe, K.J. Mutch, R.F. Tabor, J. Colloid Interface Sci. 318 (2) (2008) 244–251, http://dx.doi.org/10.1016/j.jcis.2007.10.050.
[25] S. Henderson, S. Mitchell, P. Bartlett, Colloids Surf. A: Physicochem. Eng. Aspects 190 (1–2) (2001) 81–88, http://dx.doi.org/10.1016/S0927-7757(01)00667-7.
[26] C.P. Royall, M.E. Leunissen, A. van Blaaderen, J. Phys.: Condens. Matter 15 (48) (2003) S3581–S3596, http://dx.doi.org/10.1088/0953-8984/15/48/017.
[27] M.F. Hsu, E.R. Dufresne, D.A. Weitz, Langmuir 21 (11) (2005) 4881–4887, http://dx.doi.org/10.1021/la046751m.
[28] J.W. Merrill, S.K. Sainis, E.R. Dufresne, Phys. Rev. Lett. 103 (13) (2009) 138301, http://dx.doi.org/10.1103/PhysRevLett.103.138301.
[29] M.T. Elsesser, A.D. Hollingsworth, Langmuir 26 (23) (2010) 17989–17996, http://dx.doi.org/10.1021/la1034917.
[30] R.K. Heenan, S.E. Rogers, D. Turner, A.E. Terry, J. Treadgold, S.M. King, Neutron News 22 (2) (2011) 19–21, http://dx.doi.org/10.1080/10448632.2011.569531.
[31] R.K. Heenan, J. Penfold, S.M. King, J. Appl. Cryst. 30 (6) (1997) 1140–1147, http://dx.doi.org/10.1107/S0021889897002173.
[32] G.D. Wignall, F.S. Bates, J. Appl. Cryst. 20 (1) (1987) 28–40, http://dx.doi.org/10.1107/S0021889887087181.
[33] A. Guinier, G. Fournet, Small-Angle Scattering of X-Rays, John Wiley & Sons, New York, 1955.
[34] D. Cebula, J. Goodwin, R. Ottewill, G. Jenkin, J. Tabony, Colloid Polym. Sci. 261 (7) (1983) 555–564, http://dx.doi.org/10.1007/BF01526620.
[35] I. Marković, R. Ottewill, Colloid Polym. Sci. 264 (1) (1986) 65–76, http://dx.doi.org/10.1007/BF01410309.
[36] S. Nave, J. Eastoe, R.K. Heenan, D. Steytler, I. Grillo, Langmuir 16 (23) (2000) 8741–8748, http://dx.doi.org/10.1021/la000342i.
[37] R.I. Keir, Suparno, J.C. Thomas, Langmuir 18 (5) (2002) 1463–1465, http://dx.doi.org/10.1021/la0108757.
[38] J.C. Thomas, B.J. Crosby, R.I. Keir, K.L. Hanton, Langmuir 18 (11) (2002) 4243–4247, http://dx.doi.org/10.1021/la011758e.
[39] S. Poovarodom, S. Poovarodom, J.C. Berg, J. Colloid Interface Sci. 351 (2) (2010) 415–420, http://dx.doi.org/10.1016/j.jcis.2010.07.058.
[40] M. Gacek, G. Brooks, J.C. Berg, Langmuir 28 (5) (2012) 3032–3036, http://dx.doi.org/10.1021/la204000t.
[41] K.E. Tettey, D. Lee, Soft Matter 9 (30) (2013) 7242–7250, http://dx.doi.org/10.1039/C3SM51121A.
[42] R. Cainrs, R. Ottewill, D. Osmond, I. Wagstraff, J. Colloid Interface Sci. 54 (1) (1976) 45–51, http://dx.doi.org/10.1016/0021-9797(76)90283-6.
[43] J. Eastoe, B.H. Robinson, D.C. Steytler, J. Chem. Soc., Faraday Trans. 86 (3) (1990) 511–517, http://dx.doi.org/10.1039/FT9908600511.
[44] J. Eastoe, W.K. Young, B.H. Robinson, D.C. Steytler, J. Chem. Soc., Faraday Trans. 86 (16) (1990) 2883–2889, http://dx.doi.org/10.1039/FT9908602883.
[45] B.P. Binks, H. Kellay, J. Meunier, Europhys. Lett. 16 (1) (1991) 53–58, http://dx.doi.org/10.1209/0295-5075/16/1/010.
[46] E.F. Cooper, A.-F.A. Asfour, J. Chem. Eng. Data 36 (3) (1991) 285–288, http://dx.doi.org/10.1021/je00003a008.
[47] A. Aucejo, M.C. Burguet, R. Muñoz, J.L. Marques, J. Chem. Eng. Data 40 (1) (1995) 141–147, http://dx.doi.org/10.1021/je00017a032.
[48] C. Flood, T. Cosgrove, D. Qiu, Y. Espidel, I. Howell, P. Revell, Langmuir 23 (5) (2007) 2408–2413, http://dx.doi.org/10.1021/la062034b.
[49] R. Kemp, R. Sanchez, K.J. Mutch, P. Bartlett, Langmuir 26 (10) (2010) 6967–6976, http://dx.doi.org/10.1021/la904207x.
[50] I. Marković, R.H. Ottewill, S.M. Underwood, T.F. Tadros, Langmuir 2 (5) (1986) 625–630, http://dx.doi.org/10.1021/la00071a018.

[51] Physical constants of organic compounds, in: CRC Handbook of Chemistry and Physics, 95th ed., CRC Press, 2014–2015 (Internet Version).
[52] S.M. Klein, V.N. Manoharan, D.J. Pine, F.F. Lange, Colloid Polym. Sci. 282 (1) (2003) 7–13, http://dx.doi.org/10.1007/s00396-003-0915-0.
[53] A.V. Delgado, F. González-Caballero, R.J. Hunter, L.K. Koopal, J. Lyklema, Pure. Appl. Chem. 77 (10) (2005) 1753–1805, http://dx.doi.org/10.1351/pac200577101753.
[54] N. Bjerrum, Kgl. Danske Vidensk. Selsk., Mat.-fys. Medd. 7 (9) (1926) 1–48.
[55] D.A.J. Gillespie, J.E. Hallett, O. Elujoba, A.F. Che Hamzah, R.M. Richardson, P. Bartlett, Soft Matter 10 (4) (2014) 566–577, http://dx.doi.org/10.1039/C3SM52563E.
[56] Viscosity of liquids, in: CRC Handbook of Chemistry and Physics, 95th ed., CRC Press, 2014–2015 (Internet Version).
[57] J.W. Merrill, S.K. Sainis, J. Blawzdziewicz, E.R. Dufresne, Soft Matter 6 (10) (2010) 2187–2192, http://dx.doi.org/10.1039/B926845F.
[58] S.K. Sainis, V. Germain, E.R. Dufresne, Phys. Rev. Lett. 99 (1) (2007) 018303, http://dx.doi.org/10.1103/PhysRevLett.99.018303.
[59] S.K. Sainis, V. Germain, C.O. Mejean, E.R. Dufresne, Langmuir 24 (4) (2008) 1160–1164, http://dx.doi.org/10.1021/la702432u.
[60] S.K. Sainis, J.W. Merrill, E.R. Dufresne, Langmuir 24 (23) (2008) 13334–13337, http://dx.doi.org/10.1021/la8024606.
[61] I. Grillo, in: R. Borsali, R. Pecora (Eds.), Soft Matter Characterization, Springer, Netherlands, 2008, pp. 723–782, http://dx.doi.org/10.1007/978-1-4020-4465-6_13.
[62] G.V. Schulz, Z. Phys. Chem. Abt. B 43 (1939) 25–46.
[63] S. Nave, J. Eastoe, J. Penfold, Langmuir 16 (23) (2000) 8733–8740, http://dx.doi.org/10.1021/la000341q.
[64] G.N. Smith, P. Brown, S.E. Rogers, J. Eastoe, Langmuir 29 (10) (2013) 3252–3258, http://dx.doi.org/10.1021/la400117s.
[65] O. Pekcan, M.A. Winnik, L. Egan, M.D. Croucher, Macromolecules 16 (4) (1983) 699–702, http://dx.doi.org/10.1021/ma00238a038.
[66] O. Pekcan, M.A. Winnik, M.D. Croucher, J. Colloid Interface Sci. 95 (2) (1983) 420–427, http://dx.doi.org/10.1016/0021-9797(83)90201-1.
[67] O. Pekcan, M.A. Winnik, M.D. Croucher, J. Polym. Sci.: Polym. Lett. Ed. 21 (12) (1983) 1011–1018, http://dx.doi.org/10.1002/pol.1983.130211208.
[68] A.F.M. Barton, CRC Handbook of Solubility Parameters and Other Cohesion Parameters, second ed., CRC Press, Boca Raton, Fla., 1991.
[69] J. Eastoe, Surfactant Chemistry, Wuhan University Press, Wuhan, China, 2005.